

This discussion paper is/has been under review for the journal Atmospheric Chemistry and Physics (ACP). Please refer to the corresponding final paper in ACP if available.

Physics of Stratocumulus Top (POST): turbulent mixing across capping inversion

S. P. Malinowski^{1,2}, H. Gerber³, I. Jen-LaPlante¹, M. K. Kopec¹, W. Kumala¹,
K. Nurowska¹, P. Y. Chuang⁴, D. Khelif⁵, and K. E. Haman¹

¹Institute of Geophysics, Faculty of Physics, University of Warsaw, Warsaw, Poland

²Interdisciplinary Centre for Mathematical and Computational Modelling, University of Warsaw, Warsaw, Poland

³Gerber Scientific Inc., Reston, VA, USA

⁴Earth and Planetary Sciences, University of California, Santa Cruz, CA, USA

⁵Department of Mechanical and Aerospace Engineering, University of California, Irvine, CA, USA

Received: 8 February 2013 – Accepted: 21 May 2013 – Published: 11 June 2013

Correspondence to: S. P. Malinowski (malina@fuw.edu.pl)

Published by Copernicus Publications on behalf of the European Geosciences Union.

**POST: turbulent
mixing across
capping inversion**

S. P. Malinowski et al.

Title Page

Abstract

Introduction

Conclusions

References

Tables

Figures

◀

▶

◀

▶

Back

Close

Full Screen / Esc

Printer-friendly Version

Interactive Discussion



Abstract

High spatial resolution measurements of temperature and liquid water content, accompanied by moderate resolution measurements of humidity and turbulence, collected during the Physics of Stratocumulus Top experiment are analyzed. Two thermodynamically, meteorologically and even optically different cases are investigated. An algorithmic division of the cloud top region into layers is proposed. Analysis of dynamic stability across these layers leads to the conclusion that the inversion capping the cloud and the cloud top region are turbulent due to the wind shear, which is strong enough to compensate for high static stability of the inversion. The thickness of this mixing layer adapts to wind and temperature jumps such that the gradient Richardson number stays close to its critical value. Turbulent mixing governs transport across the inversion, but the consequences of this mixing depend on the thermodynamic properties of cloud top and free troposphere. The effects of buoyancy-sorting of the mixed parcels in the cloud top region are different in conditions that permit or prevent cloud top entrainment instability. Removal of negatively buoyant air from the cloud top is observed in the first case, while buildup of the diluted cloud top layer is observed in the second one.

1 Introduction

Exchange processes between stratocumulus clouds and the free troposphere (FT) above them have been intensively investigated in many research campaigns (e.g., Albrecht et al., 1988; Lenschow et al., 1988; Stevens et al., 2003; Bretherton et al., 2004). Despite the fact that marine stratocumulus is a relatively simple system – plane-parallel, warm cloud occupying the upper part of the well mixed boundary layer above a homogeneous flat surface, and under an almost “rigid lid” temperature inversion of ~ 10 K – the understanding of entrainment into the stratocumulus topped boundary layer (STBL) is limited and estimates of the entrainment velocity are ambiguous (e.g., Stevens, 2002; Gerber et al., 2005; Faloon et al., 2005; Lilly, 2008; Carman et al.,

POST: turbulent mixing across capping inversion

S. P. Malinowski et al.

Title Page

Abstract

Introduction

Conclusions

References

Tables

Figures

◀

▶

◀

▶

Back

Close

Full Screen / Esc

Printer-friendly Version

Interactive Discussion



POST: turbulent mixing across capping inversion

S. P. Malinowski et al.

Title Page

Abstract

Introduction

Conclusions

References

Tables

Figures

◀

▶

◀

▶

Back

Close

Full Screen / Esc

Printer-friendly Version

Interactive Discussion



2012; Gerber et al., 2013). Data from in-situ measurements (e.g., Caughey et al., 1982; Nicholls, 1989; Lenschow et al., 2000; De Roode and Wang, 2007) and the results of numerical simulations (e.g., Moeng et al., 2005; Yamaguchi and Randall, 2008) clearly indicate that the top of the stratocumulus is located below the capping inversion and does not directly interact with FT above. In between there is a so-called entrainment interface layer, EIL (e.g., Caughey et al., 1982; Nicholls and Turton, 1986; Lenschow et al., 2000; Gerber et al., 2005), of thickness varying from a few meters to a few tens of meters (e.g., Haman et al., 2007; Kurowski et al., 2009).

Data from the majority of field campaigns and numerical simulations are of too poor resolution to infer the structural details of EIL and neighboring layers. However, some general conclusions concerning mixing through a stably stratified capping inversion, resulting from theoretical considerations and Large Eddy simulations (LES), indicate that in order to allow for entrainment, turbulence in the inversion must be excited. This means that at least locally the gradient Richardson number across the inversion has to exceed the critical value, as shown, e.g., by Wang et al. (2008); Kurowski et al. (2009) and Wang et al. (2012). In this paper we focus on the properties of the EIL and capping inversion in two very different cases of stratocumulus top, documented by means of high resolution measurements of velocity fluctuations, temperature and liquid water content. Airborne data analyzed here were collected during the Physics of Stratocumulus Top (POST) research campaign performed in 2008 (Gerber et al., 2010). The paper is structured in the following way: information about the POST campaign and key instruments providing data for the analysis are in Sect. 2. Two contrasting stratocumulus cases, corresponding to research flights TO10 and TO13 are presented in Sect. 3. Data analysis and discussion of the results is provided in Sect. 4, and the main findings and working hypotheses are summarized in Sect. 5.

2 POST: Physics of Stratocumulus Top research campaign

POST was a research campaign held in the vicinity of Monterey Bay in July and August 2008 (Gerber et al., 2010; Carman et al., 2012; Gerber et al., 2013). High-resolution in-situ measurements with a Center for Interdisciplinary Remotely-Piloted Aircraft Studies (CIRPAS) Twin Otter research aircraft were focused on a detailed study of processes occurring at the interface between STBL and FT. The aircraft was equipped for thermodynamics, microphysics, dynamics and radiation measurements. The adopted flight strategy was aimed at collection of data from the cloud-top region, accompanied by information on fluxes in various levels of STBL and vertical profiles of thermodynamic and dynamic parameters characterizing the lower atmosphere for the purpose of LES. Of key interest was cloud top, sampled in the course of porpoise-like flight segments across EIL, as shown in Fig. 3 of Gerber et al. (2010). In this study we focus on fine-scale measurements collected with the UFT-M thermometer (Kumala et al., 2013), Particulate Volume Monitor PVM-100 (Gerber et al., 1994), and other fast-response instruments collocated in close proximity around the radome of the aircraft (Fig. 1). The finest resolution PVM and UFT-M data discussed here are of 1000 Hz sampling frequency, which corresponds to ~ 5.5 cm spatial resolution at 55 ms^{-1} true airspeed (TAS) of the Twin Otter. Other fast response sensors provided 100 Hz and 40 Hz (corresponding to ~ 55 cm and ~ 1.4 m spatial resolution) measurements of the three components of turbulent velocity fluctuations and absolute humidity. In some flights the latter was of slightly worse resolution. Microphysical data were collected by two sets of sensors located in pods under the wings ~ 10 m from the fast sensors, producing 1 Hz (55 m spatial resolution) outputs. One of these sensors, the Phase Doppler Anemometer PDA (Chuang et al., 2008) from under the left wing is used here to characterize the microphysical properties of the investigated cases. The data is freely available from the POST database maintained by the National Center for Atmospheric Research Earth Observation Laboratory, <http://www.eol.ucar.edu/projects/post/>.

POST: turbulent mixing across capping inversion

S. P. Malinowski et al.

Title Page

Abstract

Introduction

Conclusions

References

Tables

Figures



Back

Close

Full Screen / Esc

Printer-friendly Version

Interactive Discussion



POST: turbulent mixing across capping inversion

 S. P. Malinowski et al.

[Title Page](#)
[Abstract](#)
[Introduction](#)
[Conclusions](#)
[References](#)
[Tables](#)
[Figures](#)
[⏪](#)
[⏩](#)
[◀](#)
[▶](#)
[Back](#)
[Close](#)
[Full Screen / Esc](#)
[Printer-friendly Version](#)
[Interactive Discussion](#)


Preliminary analysis of entrainment performed by Gerber et al. (2010) distinguished between two different stratocumulus regimes, classified as “classical” (8 cases) and “non-classical” (9 cases). The classical regime was characterized by a shallow and strong inversion capped by stable, dry FT. Stratocumulus cloud below was characterized by the monotonic increase of cloud liquid water content with height, like in the often quoted Fig. 4 of the review paper of Stevens (2005) or discussed in Sect. 3 of the recent review of Wood (2012), with “cloud holes” – volumes of reduced LWC – negatively buoyant and subsiding down into the cloud layer (Gerber et al., 2005, 2010; Malinowski et al., 2011). Non-classical cases show various deviations from such a picture: moist layers above the clouds, fluctuations in LWC profiles within the cloud decks, cloud holes positively buoyant and/or rising (Gerber et al., 2010, 2013; Malinowski et al., 2011). In the following we analyze details of EIL structure in classical TO10 and non-classical TO13 in order to understand similarities and differences between the behaviors of the cloud top in these two cases and to analyze details of the entrainment process.

3 Two cases: TO10 and TO13 flights

3.1 Classical case TO10

Flight TO10 was performed on 4 August 2008, 17:15–22:15 UTC. It was a daytime flight (local time was UTC –7) in a fairly uniform cloud field (c.f. satellite images in POST database). A typical sounding taken in the course of the flight (Fig. 2) shows a sharp liquid water potential temperature θ_l jump (10 K) in ~ 30 m thick layer above the cloud top, accompanied by a rapid drop of water vapor mixing ratio and a substantial wind shear ($\sim 4 \text{ m s}^{-1}$ for each horizontal component of wind velocity).

Figure 3 presents 40 Hz records of the temperature (T), liquid water content (LWC), pressure corrected altitude and fluctuations of the three components of velocity (u – the east-west component, v – the north-south component, and the vertical component w) during a typical descent into the cloud deck. A careful inspection of these plots

allows the discrimination of regions with substantially different properties, which will be quantified in Sect. 4.

The left part of the plot shows FT above the inversion, where the temperature and velocity records are smooth, fluctuations are small, and the temperature gradient is moderate. At a certain height the temperature begins to fluctuate rapidly, falling very quickly. Velocity variations show the presence of substantial wind shear and turbulence. A temperature jump of ~ 8 K is observed along the flight trajectory over a horizontal distance of ~ 550 m and a descent of ~ 12 m. Such temperature drop, wind shear, and turbulence are common features for all porpoises in this flight, suggesting the existence of a characteristic Turbulent Inversion Sub-Layer (TISL) above the cloud top.

Next the aircraft penetrates a first blob of the cloud ($LWC > 0$). Subsequent penetrations through a series of cloudy and clear filaments are characterized by remarkable (amplitude ~ 2 K) temperature fluctuations correlated with LWC. In this region horizontal velocities indicate continuing wind shear, slightly weaker than in the TISL. Turbulent velocity fluctuations are increased. Such variations are recorded over a horizontal distance of ~ 800 m in an ~ 18 m thick layer. This region is named the Cloud Top Mixing Sub-Layer (CTMSL), such that CTMSL together with TISL form the EIL. In fact we extend here a standard notion of EIL as a sublayer of the capping inversion above the cloud top moistened by former mixing events (see e.g. Gerber et al., 2005). This will be elaborated more in the following Sect. 4 of the paper.

Finally, as the temperature stabilizes, the character of the records changes. There are remarkable fluctuations of LWC, but the value at 40 Hz (~ 1.4 m spatial resolution) remains everywhere above 0. Temperature fluctuations become small, typically 0.2 K, in contrast to those in the CTMSL that exceed 2 K. Velocity fluctuations are still large, especially for the vertical component. This region is called the Cloud Top Layer (CTL).

In order to better illustrate differences between the layers of the cloud top, typical fine (1000 Hz, ~ 5.5 cm resolution) structures of LWC and T fields are presented in Fig. 4. The upper panel presents the temperature record on a ~ 200 m long segment of flight inside the TISL. Very narrow (~ 20 cm) filaments of temperature differences exceeding

POST: turbulent mixing across capping inversion

S. P. Malinowski et al.

Title Page

Abstract

Introduction

Conclusions

References

Tables

Figures



Back

Close

Full Screen / Esc

Printer-friendly Version

Interactive Discussion



**POST: turbulent
mixing across
capping inversion**

S. P. Malinowski et al.

Title Page

Abstract

Introduction

Conclusions

References

Tables

Figures



Back

Close

Full Screen / Esc

Printer-friendly Version

Interactive Discussion



1 K, indicate active turbulent mixing. The middle panel displays records of T and LWC in the CTMSL – penetrations through consecutive filaments of undiluted (maximum LWC on the porpoise) cloudy blobs; diluted, partially evaporated cloudy filaments and clear air parcels (c.f. Figs. 6–13 in Haman et al., 2007) The amplitude of temperature fluctuations within these clear air parcels is comparable to that in the TISL. Inside the undiluted and diluted cloudy filaments, the amplitude of temperature fluctuations is an order of magnitude smaller and temperature variations are not always correlated with those of LWC. Finally, in the lowest panel, records from inside the CTL on a segment with “cloud holes” present are shown for comparison. The amplitude of temperature fluctuations is ~ 0.1 K like in cloudy blobs in the CTMSL, and T and LWC fluctuations are usually correlated with few exceptions.

It is interesting to analyze vertical profiles of LWC across the CTMSL and the CTL. Plots of LWC averaged over a 1.4 m long distance (40 Hz data), as a function of height, are presented in Fig. 5 for 12 penetrations. Typically, the maximum LWC increases linearly with height, suggesting the presence of parcels lifted (almost) adiabatically from the cloud base (c.f., Pawlowska et al., 2000). Parcels with reduced LWC most often appear in the CTMSL, while in the CTL a depletion of LWC is less common and indicates the presence of “cloud holes” (Gerber et al., 2005; Kurowski et al., 2009), i.e. parcels of negative buoyancy, formed in the course of mixing and evaporative cooling at the cloud top, slowly descending across the cloud deck.

Figure 6 shows in-cloud vertical profiles of median cloud microphysical properties averaged for the entire flight on this day. Observations are from the phase-Doppler interferometer and are binned by altitude for each individual slant ascent or descent relative to the cloud top for that ascent or descent profile using a threshold of 0.05 g kg^{-1} . On this day, the median (or 50th percentile) drop diameter generally increases slowly with altitude, ranging from $15 \mu\text{m}$ at an altitude of 100 m below cloud top to nearly $17 \mu\text{m}$ right at cloud top. This same slow increase in drop size is also found for other percentiles of the drop distribution. The breadth of the number size distribution thus is generally quite similar in this portion of the cloud. The drop number concentration

is reasonably constant with altitude (between 100 and 120 mg⁻¹) given that the average standard deviation in drop concentration for each altitude is 11 mg⁻¹. Overall, the microphysical observations indicate a fairly well-mixed cloud whose properties are dominated mainly by condensational growth and do not exhibit any strong signs of entrainment effects. It is possible that the decrease in drop number concentration in the top 10 m of the cloud indicates a modest amount of inhomogeneous mixing, but, as mentioned earlier, the effect is within the range of uncertainty.

3.2 Non-classical case TO13

Meteorological conditions during evening flight TO13 (performed 9 August 2008, 00:58–06:00 UTC) were different from the ones during TO10 (Fig. 7). While the total jump of θ_1 between the middle of the mixed layer and the ~ 1000 m altitude is comparable to the TO10 case, the sharp inversion above the cloud top has a temperature jump of no more than ~ 4 K (in many penetrations this temperature jump was as weak as ~ 1 K). θ_1 and total water profiles are deflected from vertical across the ~ 80 m thick region in the upper part of the cloud. This suggests that this region is dynamically decoupled from the mixed atmospheric boundary layer. The mixing ratio above the cloud top is high. Figure 7 shows fluctuations of humidity and an almost saturated layer at ~ 750 m height. In many penetrations conditions close to saturation were present in a thick layer above the cloud top. The wind jump in the cloud top region is smaller than in the TO10 case and the shear layer is significantly deeper. Its bottom correlates with the top of the mixed boundary layer. There is also a substantial variability of the shear layer among the penetrations.

In Fig. 8, 40 Hz time series of T , LWC, altitude, and velocity fluctuations in a typical penetration of the cloud top during flight TO13 are presented. In contrast to the TO10 case shown previously in Fig. 3, the beginning of the temperature inversion and increased fluctuations discriminating FT and TISL are less distinct. The beginning of CTMSL is again diagnosed with a first blob of cloudy air. There are increased velocity

POST: turbulent mixing across capping inversion

S. P. Malinowski et al.

Title Page

Abstract

Introduction

Conclusions

References

Tables

Figures



Back

Close

Full Screen / Esc

Printer-friendly Version

Interactive Discussion



**POST: turbulent
mixing across
capping inversion**

S. P. Malinowski et al.

Title Page

Abstract

Introduction

Conclusions

References

Tables

Figures



Back

Close

Full Screen / Esc

Printer-friendly Version

Interactive Discussion



fluctuations associated with this blob and successive cloud volumes. Except for the first cloudy filaments, LWC in CTMSL only slowly approaches the maximum LWC in the CTL below. This suggests that cloud filaments in this region do not contain adiabatic parcels originating at the cloud base, which again suggests decoupling from the mixed boundary layer. Humidity in both cloud and clear air filaments approaches the saturation value. In contrast to the TO10 case, fluctuations of T , LWC, and all velocity components continue, with little change to mark the border between CTMSL and CTL.

The fine scale structure of successive layers of stratocumulus top is shown in Fig. 9. Again, large fluctuations of T are observed in TISL, indicating turbulent mixing. The amplitude of these fluctuations is smaller than in TO10 in accordance with the smaller temperature jump across the inversion. In CTMSL diluted cloudy blobs (reduced LWC) prevail, and there are not so many clear air filaments as in TO10. This is in agreement with the high humidity of FT and TISL, which prevents the mixed cloud parcels from rapid evaporation. Regions of reduced LWC are broader and the borders are less sharp. T and LWC records in CTL are correlated, again with few exceptions.

In Fig. 10 twelve typical vertical profiles of LWC are presented in a similar manner to Fig. 5. The difference between TO13 and TO10 is striking. In TO13 the maximum value of LWC in the cloud top region decreases or is constant with height. Additionally, several panels in Fig. 10 suggest that the layer with decreasing maximum LWC tops a layer with the typical (for stratocumulus clouds) linear increase of the maximum LWC with altitude. It is worth mentioning that such a profile of LWC in stratocumulus top is not unique. It resembles, e.g. RF08B case of FIRE I campaign (c.f. Fig. 6 in De Roode and Wang, 2007).

Figure 11 shows averaged cloud microphysical property profiles for Flight TO13. In contrast with Fig. 6, on this day the drop diameters are larger than on TO10 by almost $10\ \mu\text{m}$, with median drop sizes around 24 to $26\ \mu\text{m}$. The median drop diameter also appears to be quite constant with altitude in the top 60 m of the cloud (between -60 and $0\ \text{m}$) rather than slowly increasing as in TO10. The drop size distribution broadens towards smaller sizes as altitude increases in this same region, as evidenced by

**POST: turbulent
mixing across
capping inversion**

S. P. Malinowski et al.

Title Page

Abstract

Introduction

Conclusions

References

Tables

Figures

◀

▶

◀

▶

Back

Close

Full Screen / Esc

Printer-friendly Version

Interactive Discussion



the decreases in the 10th and 25th percentile drop diameters. Drop number concentration in Fig. 11 generally decreases with altitude, from around 50 mg^{-1} at 120 m below cloud top down to 20 mg^{-1} right at cloud top. These profiles are consistent with a poorly-mixed or decoupled cloud top region. Entrainment and mixing appears to both decrease drop concentration, by dilution and potentially by complete evaporation of drops, as well as cause some drops to partially shrink in size. High humidity of entrained air would be expected to decrease number concentration to a much larger degree than drop size, also consistent with the observations.

One contributor to the median drop size remaining constant near cloud top in response to entrainment may be that collisional growth is also active in this cloud. The size distribution at the large diameter side extends to fairly large sizes (90th percentile diameter around $32 \mu\text{m}$), which is most likely caused by collisional growth. Intermittent drizzle is also much stronger on this day as compared with TO10, consistent with the larger drop sizes.

4 Data analysis and discussion

The previous section documents substantial differences between the “classical” TO10 and “non classical” TO13 stratocumulus cases. These differences in thermodynamical, microphysical and dynamical properties of stratocumulus tops were reflected in the visual appearance of the clouds. Observers onboard the aircraft reported “classic stratocumulus layer” in the course of TO10, in contrast to “cloud tops looking like moguls,” i.e., the bumps on a ski slope, in TO13. Clearly, the nature of differences require deeper insight into the data.

4.1 Layer division

Detailed analysis of all porpoises in data from the two flights showed that in the majority of recorded cases a division into similar cloud top sublayers is possible. Testing various

POST: turbulent mixing across capping inversion

S. P. Malinowski et al.

Title Page

Abstract

Introduction

Conclusions

References

Tables

Figures

◀

▶

◀

▶

Back

Close

Full Screen / Esc

Printer-friendly Version

Interactive Discussion



criteria led to a quantitative definition of the division. In addition to LWC, the criteria take into account the gradient of liquid water potential temperature, $\Delta\theta_l/\Delta z$; the turbulent kinetic energy, TKE; and the square of the horizontal wind shear, $(\Delta u/\Delta z)^2 + (\Delta v/\Delta z)^2$, obtained as the sum of squares of the horizontal velocity deviations relative to the top of each porpoise. Calculations of TKE and the horizontal wind shear use a moving average of 300 points from the 40 Hz data. $\Delta\theta_l/\Delta z$ is calculated from a linear fit of the liquid water potential temperature over the same interval. The averaging length corresponds to a distance of ~ 450 m, chosen to average across a few large turbulent eddies, with a typical size of ~ 100 m. On the other hand, given the 1.5 m s^{-1} ascent/descent rate, such averaging allows distinguishing between layers of thickness ~ 10 m. All three properties are illustrated for a segment from each flight in Figs. 12 and 13.

In these figures the sublayers are delineated by three vertical black lines. From left to right, the first line shows the separation between FT and TISL, which is identified as the top of capping inversion, i.e., highest point where $\Delta\theta_l/\Delta z$ exceeds 0.2 K m^{-1} and simultaneously TKE exceeds $0.01 \text{ m}^2 \text{ s}^{-2}$. Next the division between TISL and CTMSL corresponds to the uppermost point where LWC exceeds 0.05 g m^{-3} , as shown for the same flight segments in Figs. 3 and 8. The final division between CTMSL and CTL is determined by the point where the square of the horizontal wind shear reaches 90% of maximum.

For the descending segment of flight TO10 shown in Fig. 12, the division between FT and TISL occurs at about 67 727 s (656 m altitude). Here the temperature begins to fluctuate rapidly, while decreasing. The turbulent kinetic energy remains high throughout the TISL. Next comes the first indication of CTMSL at 67 736 s (644 m altitude), where the temperature is becoming more stable and turbulent kinetic energy is decreasing. This is followed by CTL at 67 748 s (626 m altitude). From this point LWC stays above zero, while the temperature, turbulent kinetic energy, and horizontal wind stabilize.

As noted, the layers are less distinct in flight TO13 than in TO10. Divisions using these criteria were possible for about half of all segments in this flight. For the segment shown in Fig. 13, the division between FT and TISL occurs at about 18 184 s (730 m

altitude) and coincides with the occurrence of very small, rapid T fluctuations. CTMSL begins at 18 211 s (663 m altitude) with the first distinct cloud blob and continues for much of the penetration. Both TISL and CTMSL show significant variation of $\Delta\theta_i/\Delta z$, in contrast to the distinct maximum in TISL for flight TO10. Finally at 18 291 s (536 m altitude) the CTL is reached and the horizontal wind plateaus. The layers are notably thicker in this case, with a TISL thickness of 67 m and CTMSL thickness of 127 m compared to 12 m and 18 m, respectively, for flight TO10.

4.2 Richardson number

Using the divisions just described, the bulk Richardson number is estimated for each layer according to the following formula:

$$R_i = \frac{\frac{g}{\theta} \left(\frac{\Delta\theta}{\Delta z} \right)}{\left(\frac{\Delta u}{\Delta z} \right)^2 + \left(\frac{\Delta v}{\Delta z} \right)^2} \quad (1)$$

where g is the acceleration due to gravity, and $\Delta\theta$, Δu and Δv are the jumps of potential temperature and horizontal velocity components across the thickness of the layer Δz . Note, that this is a crude estimate of R_i , subject to uncertainties due to the measurements along an inclined trajectory, deflections of the cloud top from plane-parallel structure and possible non-stationarity of cloud processes. Nevertheless, we believe that statistics of R_i estimates from a vast number of cloud top penetrations provide us at least qualitative insight into the properties of turbulence in the vicinity of cloud top.

Figure 14 shows histograms of R_i values estimated on porpoises of flight TO10 in the consecutive layers: the lower ~ 50 m of FT (top left), TISL (top right), CTMSL (middle left), CTL (middle right) and EIL (combination of TISL and CTMSL, bottom). The sampled thickness of FT and CTL varies across segments due to differences in the turnaround between ascending and descending segments, or vice-versa, relative to the cloud. This can affect the Richardson number observed across those partial layers.

Title Page

Abstract

Introduction

Conclusions

References

Tables

Figures

◀

▶

◀

▶

Back

Close

Full Screen / Esc

Printer-friendly Version

Interactive Discussion



Flight segments where the calculated Richardson number fell outside the range $[-2, 8]$, or where the layers were not identified, are not included in the histograms.

Recalling many studies (see, e.g., recent discussions in Galperin et al., 2007; Grachev et al., 2012), values of $R_i > 1$ suggest stably stratified, non-turbulent fluid.

While $R_{iC} = 0.25$ is usually considered a critical value, in the range of $0.25 < R_i < 1$ turbulence is often observed. Positive values $0 < R_i < 0.25$ correspond to fully turbulent, stably stratified fluid, while $R_i < 0$ indicate statically unstable fluid. Keeping the above in mind, the two upper panels of Fig. 14 indicate that FT is stably stratified and mostly non-turbulent. In contrast TISL, characterized by increased static stability is marginally turbulent: estimates of R_i from all penetrations peak narrowly in the three highlighted bins centered at 0.25, 0.50 and 0.75. R_i histograms from CTMSL and CTL require more discussion. First, the median values of R_i in CTMSL and CTL indicate turbulence. There are also signatures of $R_i < 0.25$ in both layers and $R_i < 0$ in CTL. Second, from the vertical sounding and the definition of R_i it follows that R_i estimates in CTL and in some penetrations of CTMSL come from small differences in horizontal wind and θ . Thus, they are associated with large errors resulting from the division of two small numbers. This can be verified in Fig. 12, where the gradient of θ_1 (not very different from the gradient of θ) and the horizontal wind across these layers had very small values. Similar reasoning explains the observed variability of R_i estimates in FT: the wind shear in this layer is small, especially in the case of shallow penetration into FT in the course of a porpoise.

The last histogram of R_i in Fig. 14 allows the characterization of the whole EIL. This estimate is more reliable, since the division between TISL and CTMSL in each porpoise is affected by random error due to inherent variability in the height of the top-most cloud blob. It is also the closest to the canonical interpretation of R_i , i.e., the ratio of potential to kinetic energies across the whole depth of the shear layer. Clearly, the values of R_i indicate that EIL is marginally turbulent.

Figure 15 presents histograms of R_i for the TO13 case. In general, the distributions are quite similar to those from TO10. The statistics are limited since only about half the

POST: turbulent mixing across capping inversion

S. P. Malinowski et al.

Title Page

Abstract

Introduction

Conclusions

References

Tables

Figures

◀

▶

◀

▶

Back

Close

Full Screen / Esc

Printer-friendly Version

Interactive Discussion



POST: turbulent mixing across capping inversion

S. P. Malinowski et al.

Title Page

Abstract

Introduction

Conclusions

References

Tables

Figures

◀

▶

◀

▶

Back

Close

Full Screen / Esc

Printer-friendly Version

Interactive Discussion



flight segments had well-identified layers, as discussed in the previous section. Weaker temperature gradients across TISL result in the larger uncertainty of R_i determination. However, a vast majority of the cases in both TISL and CTMSL fall into three bins centered at 0.25, 0.50 and 0.75, indicating marginally turbulent layers. This is also true for the whole EIL.

4.3 A conceptual model of Sc top

A surprisingly consistent picture of the cloud top region dynamics emerges from the analysis of the two very different cases. The free troposphere above the inversion is statically and dynamically stable. Values of $R_i > 1$ suggest no turbulence, which is consistent with the appearance of the velocity and temperature records. The layers below: TISL, CTMSL and their combination – EIL, are turbulent, with $R_i \approx R_{iC}$ indicating closeness to the margin of stability. Frequent sharp fluctuations of temperature, LWC and all velocity components demonstrate the presence of intensive mixing. It shall be underlined that despite the maximum static stability across TISL, the inversion is turbulent and the border between non-turbulent FT and turbulent TISL is sharp since no gradual variation of small-scale velocity fluctuations with height is observed. The location of this border coincides with the upper limit of the wind shear layer. This is also in agreement with a generic concept of entrainment as “the mean inflow across the edge of a turbulent flow” (see the review paper by Turner, 1986).

How can such a consistent picture of EIL emerge, despite different temperature and velocity jumps, visual appearances of clouds and thermodynamic properties of cloud tops? Consider the formula for R_i , rewritten as:

$$R_i = \left(\frac{g}{\theta} \right) \frac{\Delta\theta}{\Delta u^2 + \Delta v^2} \Delta z \quad (2)$$

Remember that forcings responsible for temperature and velocity jumps across EIL (TISL), $\Delta\theta$, Δu , Δv , assuming convectively well mixed STBL are: radiative cooling at the cloud top, large scale subsidence, advection and horizontal pressure gradient. The

POST: turbulent mixing across capping inversion

S. P. Malinowski et al.

Title Page

Abstract

Introduction

Conclusions

References

Tables

Figures

◀

▶

◀

▶

Back

Close

Full Screen / Esc

Printer-friendly Version

Interactive Discussion



only local parameter is layer thickness, Δz . Observed $R_i \approx R_{iC}$ across EIL (TISL) suggests a dynamical adaptation of Δz to forcings. This suggestion, formulated in a stratocumulus context by Katzwinkel et al. (2011); is well documented in oceanic statically stable shear layers, (see Smyth and Moum, 2000, c.f. Figs. 11 and 12 therein or the review paper by Peltier and Caufield, 2003). If confirmed, this finding paves the road to entrainment/mixing parametrization based on properties of turbulence in TISL along the reasoning of Pham and Sarkar (2010).

Now the second problem needs explanation: why, despite such strong similarities in dynamics, are the cloud tops in TO10 and TO13 so different? Analysis of mixing diagrams indicates that thermodynamic properties of CTL and FT in TO10 allow cloud top entrainment instability (CTEI): uniform mixtures of air from the cloud top and above the EIL of fraction $\chi < 0.12$ of clear air are negatively buoyant and only those of fraction $\chi < 0.11$ are saturated after mixing. Independent analyses of buoyancy reversal and mixing fraction performed by Gerber et al. (2013) confirm CTEI in TO10. In such case mixed cloudy parcels of reduced LWC (and some clear parcels close to saturation) are quickly removed from the CTMSL due to the action of negative buoyancy. Thus, cloudy parcels in the CTMSL are almost unmixed, with relatively narrow droplet spectra and high LWC. Mixed clear air parcels, of increased temperature and humidity, contribute to the thickness of the TISL and undergo consecutive mixing events in turbulent inversion.

In contrast, the conditions during TO13 are CTEI prohibiting. Mixing of air from the CTL with humid, only slightly warmer air from the FT cannot reverse buoyancy. Mixtures of as high a fraction of clear air as $\chi < 0.7$ are still cloudy (with reduced LWC and droplet concentration) and positively buoyant (again in agreement with Gerber et al., 2013). The majority of mixed parcels maintaining cloud water remain close to the level where mixing occurred, undergoing secondary mixing events. Inhomogeneous mixing is more likely in the humid environment (see, e.g., analysis of characteristic times of mixing and evaporation in Andrejczuk et al., 2009) and leads to the reduced sizes of small droplets, while the long residence time of cloudy parcels in highly turbulent CTMSL may lead to formation of larger droplets due to collision-coalescence processes.

POST: turbulent mixing across capping inversion

S. P. Malinowski et al.

Title Page

Abstract

Introduction

Conclusions

References

Tables

Figures

◀

▶

◀

▶

Back

Close

Full Screen / Esc

Printer-friendly Version

Interactive Discussion



Taking into account the above analysis, the structure and phenomenology of stratocumulus top can be summarized graphically in Fig. 16. STBL is capped by non-turbulent free troposphere. Within STBL air is well mixed due to the action of large convective eddies spanning the whole STBL depth (indicated in the cartoon as thick brown arrows). The entrainment interface layer is turbulent (curved brown arrows). Turbulence is kept at a level close to the dynamic equilibrium resulting from production by the wind shear (straight brown arrows) and damping by the strong static stability (green profile of θ_1) by the self-adapting thickness of the EIL.

The effects of turbulent mixing depend on the thermodynamical properties of FT and CTL. In a CTEI permitting situation these mixed and homogenized parcels which are cloudy or close to saturation are removed from CTMSL by negative buoyancy. The remaining homogenized clear air parcels are subject to secondary mixing events and are incorporated into TISL or form clear air volumes encompassed by cloudy volumes in CTMSL. The removal mechanism is efficient enough to keep CTMSL relatively thin, despite ongoing mixing across TISL. In a CTEI prohibiting situation, mixed cloudy parcels are not effectively removed from CTMSL. The thickness of this layer grows (red double arrows in the cartoon) and it is occupied mostly by diluted cloudy parcels and almost saturated clear air blobs, which alters profiles of LWC (blue lines, solid and dashed).

Certainly, this is a simplified picture of the cloud top emerging from analysis of dynamics and thermodynamics only, and shall be expanded in future. Changes in the profiles of LWC affect radiative transport and, in effect, influence temperature. Droplet collisions in CTMSL, probably after some time, trigger water removal from CTMSL by drizzle. Nevertheless, this conceptual model is a step towards untangling a highly complicated problem of entrainment into STBL.

5 Conclusions

High-resolution airborne measurements performed in the course of the POST research campaign allow the division of the cloud top region into layers: non turbulent free tro-

POST: turbulent mixing across capping inversion

S. P. Malinowski et al.

Title Page

Abstract

Introduction

Conclusions

References

Tables

Figures



Back

Close

Full Screen / Esc

Printer-friendly Version

Interactive Discussion



posphere, turbulent capping inversion sublayer, turbulent cloud top mixing sublayer (both forming the Entrainment Interface Layer) and the cloud layer below. Two, thermodynamically and microphysically different cases of stratocumulus cloud investigated here show a rather consistent picture of the dynamics. (1) Exchange between the free troposphere and cloud top is governed by turbulent mixing across the inversion. The thickness of the inversion and adjacent cloud top mixing sublayer results from dynamic adaptation to temperature (density) and wind jumps between CTL and FT (considered here as external factors). Adaptation means here maintaining the Richardson number across EIL close to its critical value. (2) Effects of the exchange depend on thermodynamic properties of air masses undergoing mixing. When temperature and moisture jumps permit cloud top entrainment instability, negatively buoyant mixed parcels are removed from CTMSL region due to negative buoyancy. Resulting CTMSL is thin and cloudy parcels in this layer are almost undiluted. In the CTEI preventing case, mixed parcels often remain cloudy and buoyancy sorting causes them to remain in the cloud top region below inversion, making CTMSL thick. Cloudy parcels in this sublayer exhibit widened droplet spectra and a reduced LWC and droplet number condensation.

Decomposition of the entrainment-mixing process into dynamically driven turbulent mixing across the inversion and the thermodynamical effect of mixing gives a perspective on new entrainment parameterizations, accounting for the efficiency of mixing across a stably stratified turbulent shear layer (Pham and Sarkar, 2010) and the subsequent thermodynamic effects of mixing.

The last remark concerns STBL capped with inversion without wind shear. What mechanism is responsible for mixing across a very stable inversion layer? The answer is given in Kurowski et al. (2009), who modeled such a situation, based on the DY-COMS II RF01 case. They found, that the organized updrafts in STBL have a kinetic energy far too small to penetrate the inversion and, instead, diverge just below it. This diverging outflow produces shear, capable of inducing turbulence and mixing across the EIL. Figures 7 and 9 in that paper present the details of this process and subsequent removal of mixed parcels by negative buoyancy (CTEI permitting situation).

POST: turbulent mixing across capping inversion

S. P. Malinowski et al.

Title Page

Abstract

Introduction

Conclusions

References

Tables

Figures

◀

▶

◀

▶

Back

Close

Full Screen / Esc

Printer-friendly Version

Interactive Discussion



Acknowledgements. POST field project was supported by the National Science Foundation with the grant ATM- 0735121 and by the Polish Ministry of Science and Higher Education with the grant 186/W-POST/2008/0. We thank all POSTers and CIRPAS for the excellent collaboration during the field campaign. In particular we acknowledge Halfidi Jonsson who provided CIRPAS data into the POST database and Steven Krueger for inspiring discussions. Analyses presented here were supported by the Department of the Navy Grant N62909-11-1-7061 issued by Office of Naval Research Global (J-LP and MK) and Polish PROZA POIG.010301-00/140/08 (SPM) project. SPM acknowledges the “Nature of Turbulence” program at the Kavli Institute for Theoretical Physics, interactions in the course of the program helped to understand cloud top phenomenology. The United States Government has a royalty-free license throughout the world in all copyrighable material contained herein.

References

- Albrecht, B. A., Randall, D. A., and Nicholls, S.: Observations of marine stratocumulus clouds during FIRE, *B. Am. Meteorol. Soc.*, 69, 618–626, doi:10.1175/1520-0477(1988)069<0618:OOMSCD>2.0.CO;2, 1988. 15234
- Andrejczuk, M., Grabowski, W. W., Malinowski, S. P., and Smolarkiewicz, P. K.: Numerical simulation of cloud-clear air interfacial mixing: homogeneous versus inhomogeneous mixing, *J. Atmos. Sci.*, 66, 2493–2500, doi:10.1175/2009JAS2956.1, 2009. 15247
- Bretherton, C. S., Uttal, T., Fairall, C. W., Yuter, S. E., Weller, R. A., Baumgardner, D., Comstock, K., Wood, R., and Raga, G. B.: The epic 2001 stratocumulus study, *B. Am. Meteorol. Soc.*, 85, 967–977, doi:10.1175/BAMS-85-7-967, 2004. 15234
- Carman, J. K., Rossiter, D. L., Khelif, D., Jonsson, H. H., Faloon, I. C., and Chuang, P. Y.: Observational constraints on entrainment and the entrainment interface layer in stratocumulus, *Atmos. Chem. Phys.*, 12, 11135–11152, doi:10.5194/acp-12-11135-2012, 2012. 15234, 15236
- Caughey, S. J., Crease, B. A., and Roach, W. T.: A field study of nocturnal stratocumulus: 2. Turbulence structure and entrainment, *Q. J. Roy. Meteor. Soc.*, 108, 125–144, doi:10.1002/qj.49710845508, 1982. 15235

POST: turbulent mixing across capping inversion

S. P. Malinowski et al.

Title Page

Abstract

Introduction

Conclusions

References

Tables

Figures

◀

▶

◀

▶

Back

Close

Full Screen / Esc

Printer-friendly Version

Interactive Discussion



- Chuang, P. Y., Saw, E. W., Small, J. D., Shaw, R. A., Sipperley, C. M., Payne, G. A., and Bachalo, W. D.: Airborne phase Doppler interferometry for cloud microphysical measurements, *Aerosol Sci. Tech.*, 42, 685–703, doi:10.1080/02786820802232956, 2008. 15236
- De Roode, S. R. and Wang, Q.: Do stratocumulus clouds detrain? FIRE I data revisited, *Bound.-Lay. Meteorol.*, 122, 479–491, doi:10.1007/s10546-006-9113-1, 2007. 15235, 15241
- Faloon, I., Lenschow, D. H., Campos, T., Stevens, B., and van Zanten, M.: Observations of entrainment in Eastern Pacific marine stratocumulus using three conserved scalars, *J. Atmos. Sci.*, 62, 3268–3285, doi:10.1175/JAS3541.1, 2005. 15234
- Galperin, B., Sukoriansky, S., and Anderson, P. S.: On the critical Richardson number in stably stratified turbulence, *Atmos. Sci. Lett.*, 8, 65–69, doi:10.1002/asl.153, 2007. 15245
- Gerber, H.: Microphysics of marine stratocumulus clouds with two drizzle modes, *J. Atmos. Sci.*, 53, 1649–1662, doi:10.1175/1520-0469(1996)053<1649:MOMSCW>2.0.CO;2, 1996.
- Gerber, H., Arends, B. G., and Ackerman, A. S.: A new microphysics sensor for aircraft use, *Atmos. Res.*, 31, 235–252, doi:10.1016/0169-8095(94)90001-9, 1994. 15236
- Gerber, H., Frick, G., Malinowski, S. P., Brenguier, J.-L., and Burnet, F.: Holes and entrainment in stratocumulus, *J. Atmos. Sci.*, 62, 443–459, doi:10.1175/JAS-3399.1, 2005. 15234, 15235, 15237, 15238, 15239
- Gerber, H., Frick, G., Malinowski, S. P., Kumala, W., and Krueger, S.: POST – A New Look at Stratocumulus, 13th Conference on Cloud Physics, Portland, OR, 2010, American Meteorological Society, available at: <http://ams.confex.com/ams/pdfpapers/170431.pdf> (last access: 10 June 2013), 2010. 15235, 15236, 15237
- Gerber, H., Frick, G., Malinowski, S. P., Jonsson, H., Khelif, D., and Krueger, S.: Entrainment rates and microphysics in POST stratocumulus, *J. Geophys. Res.*, submitted, 2013. 15235, 15236, 15237, 15247
- Grachev, A. A., Andreas, E. L., Fairall, C. W., Guest, P. S., and Persson, O. G.: The critical Richardson number and limits of applicability of local similarity theory in the stable boundary layer, *Bound.-Lay. Meteorol.*, 47, 51–83, doi:10.1007/s10546-012-9771-0, 2013. 15245
- Haman, K. E., Malinowski, S. P., Kurowski, M. J., Gerber, H., and Brenguier, J.-L.: Small scale mixing processes at the top of a marine stratocumulus – a case study, *Q. J. Roy. Meteorol. Soc.*, 133, 213–226, doi:10.1002/qj.5, 2007. 15235, 15239
- Katzwinkel, J., Siebert, H., and Shaw, R. A.: Observation of a self-limiting, shear-induced turbulent inversion layer above marine stratocumulus, *Bound.-Lay. Meteorol.*, 145, 131–143, doi:10.1007/s10546-011-9683-4, 2011. 15247

POST: turbulent mixing across capping inversion

S. P. Malinowski et al.

Title Page

Abstract

Introduction

Conclusions

References

Tables

Figures

◀

▶

◀

▶

Back

Close

Full Screen / Esc

Printer-friendly Version

Interactive Discussion



Kumala, W., Haman, K. E., Kopec, M. K., Khelif, D., and Malinowski, S. P.: Modified Ultrafast Thermometer UFT-M and temperature measurements during Physics of Stratocumulus Top (POST), *Atmos. Meas. Tech. Discuss.*, 6, 2085–2112, doi:10.5194/amtd-6-2085-2013, 2013. 15236

5 Kurowski, M. J., Malinowski, S. P., and Grabowski, W. W.: A numerical investigation of entrainment and transport within a stratocumulus-topped boundary layer, *Q. J. Roy. Meteorol. Soc.*, 135, 77–92, doi:10.1002/qj.354, 2009. 15235, 15239, 15249

Lenschow, D. H., Paluch, I. R., Brandy, A. R., Pearson, R., Kawa, S. R., Weaver, C. J., Kay, J. G., Thornton, D. C., and Driedger, A. R.: Dynamics and Chemistry of Marine Stratocumulus (DYCOMS) experiment, *B. Am. Meteorol. Soc.*, 69, 1058–1067, doi:10.1175/1520-0477(1988)069<1058:DACOMS>2.0.CO;2, 1988. 15234

Lenschow, D. L., Zhou, M., Zeng, X., Chen, L., and Xu, X.: Measurements of fine-scale structure at the top of marine stratocumulus, *Bound.-Lay. Meteorol.*, 97, 331–357, doi:10.1023/A:1002780019748, 2000. 15235

15 Lilly, D. K.: Validation of a mixed-layer closure. II: observational tests, *Q. J. Roy. Meteorol. Soc.*, 134, 57–67, doi:10.1002/qj.183, 2008. 15234

Malinowski, S. P., Haman, K. E., Kopec, M. K., Kumala, W., and Gerber, H.: Small-scale turbulent mixing at stratocumulus top observed by means of high resolution airborne temperature and LWC measurements, *J. Phys. Conf. Ser.*, 318, 072013, doi:10.1088/1742-6596/318/7/072013, 2011. 15237

Moeng C-H., Stevens, B., and Sullivan, P. P.: Where is the interface of the stratocumulus-topped PBL?, *J. Atmos. Sci.*, 62, 2626–2631, doi:10.1175/JAS3470.1, 2005. 15235

Nicholls, S.: The structure of radiatively driven convection in stratocumulus, *Q. J. Roy. Meteorol. Soc.*, 115, 487–511, doi:10.1002/qj.49711548704, 1989. 15235

25 Nicholls, S. and Turton, J. D.: An observational study of the structure of stratiform cloud sheets: Part 2: Entrainment, *Q. J. Roy. Meteorol. Soc.*, 112, 461–480, doi:10.1002/qj.49711247210, 1986. 15235

Pawlowska, H., Brenguier, J-L., and Burnet, F.: Microphysical properties of stratocumulus clouds, *Atmos. Res.*, 55, 15–23, doi:10.1016/S0169-8095(00)00054-5, 2000. 15239

30 Peltier, W. R. and Caulfield, C. P.: Mixing Efficiency in stratified shear flows, *Annu. Rev. Fluid. Mech.*, 35, 135–167, doi:10.1146/annurev.fluid.35.101101.161144, 2003. 15247

Pham, H. T. and Sarkar, S.: Transport and mixing of density in a continuously stratified shear layer, *J. of Turbul.*, 11, 1–23, doi:10.1080/14685248.2010.493560, 2010. 15247, 15249

POST: turbulent mixing across capping inversion

S. P. Malinowski et al.

Title Page

Abstract

Introduction

Conclusions

References

Tables

Figures

◀

▶

◀

▶

Back

Close

Full Screen / Esc

Printer-friendly Version

Interactive Discussion



- Smyth, W. D. and Moum, J. N.: Length scales of turbulence in stably stratified mixing layers, *Phys. Fluids*, 12, 1327–1342, doi:10.1063/1.870385, 2000. 15247
- Stevens, B.: Entrainment in stratocumulus-topped mixed layers, *Q. J. Roy. Meteorol. Soc.*, 128, 2663–2690, doi:10.1256/qj.01.202, 2002. 15234
- 5 Stevens, B.: Atmospheric moist convection, *Annu. Rev. Earth. Pl. Sc.*, 33, 605–643, doi:10.1146/annurev.earth.33.092203.122658, 2005. 15237
- Stevens, B., Lenschow, D. H., Vali, G., Gerber, H., Bandy, A., Blomquist, B., Brenguier, J-L., Bretherton, C. S., Burnet, F., Campos, T., Chai, S., Faloon, I., Friesen, D., Haimov, S., Laursen, K., Lilly, D. K., Loehrer, S. M., Malinowski, S. P., Morley, B., Petters, M. D.,
 10 Rogers, D. C., Russell, L., Savic-Jovicic, V., Snider, J. R., Straub, D., Szumowski, M. J., Takagi, H., Thornton, D. C., Tschudi, M., Twohy, C., Wetzell, M., and van Zanten, M. C.: Dynamics and chemistry of marine stratocumulus – Dycoms II, *B. Am. Meteorol. Soc.*, 84, 579–593, doi:10.1175/BAMS-84-5-579, 2003. 15234
- Turner, J. S.: Turbulent entrainment: the development of the entrainment assumption, and its application to geophysical flows, *J. Fluid. Mech.*, 173, 431–471, doi:10.1017/S0022112086001222, 1986. 15246
- 15 Wang, S., Golaz, J.-C., and Wang, Q.: Effect of intense wind shear across the inversion on stratocumulus clouds, *Geophys. Res. Lett.*, 35, L15814., doi:10.1029/2008GL033865, 2008. 15235
- 20 Wang, S., Zheng, X., and Jiang, Q.: Strongly sheared stratocumulus convection: an observationally based large-eddy simulation study, *Atmos. Chem. Phys.*, 12, 5223–5235, doi:10.5194/acp-12-5223-2012, 2012. 15235
- Wood, R.: Stratocumulus clouds, *Mon. Weather Rev.*, 140, 2373–2423, doi:10.1175/MWR-D-11-00121.1, 2012. 15237
- 25 Yamaguchi, T. and Randall, D. A.: Large-Eddy simulation of evaporatively driven entrainment in cloud-topped mixed layers, *J. Atmos. Sci.*, 65, 1481–1504, doi:10.1175/2007JAS2438.1, 2008. 15235



Fig. 1. Radome of CIRPAS Twin Otter research aircraft with fast-response instruments used in POST.

ACPD

13, 15233–15269, 2013

POST: turbulent mixing across capping inversion

S. P. Malinowski et al.

Title Page

Abstract

Introduction

Conclusions

References

Tables

Figures

◀

▶

◀

▶

Back

Close

Full Screen / Esc

Printer-friendly Version

Interactive Discussion



POST: turbulent mixing across capping inversion

S. P. Malinowski et al.

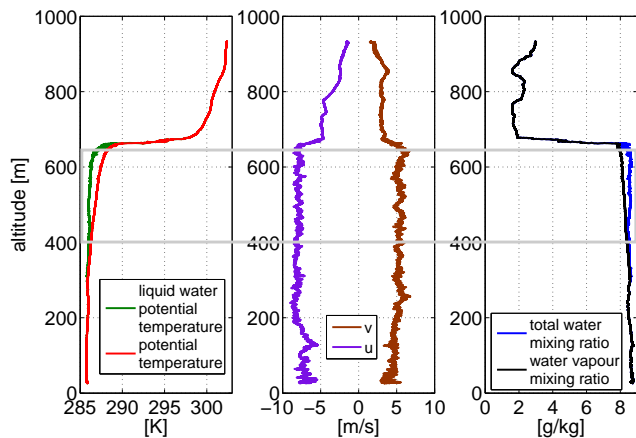


Fig. 2. Vertical profiles of potential temperatures, components of horizontal wind, and mixing ratios characteristic for research flight TO10. Cloud layer marked with a gray box.

[Title Page](#)[Abstract](#)[Introduction](#)[Conclusions](#)[References](#)[Tables](#)[Figures](#)[◀](#)[▶](#)[◀](#)[▶](#)[Back](#)[Close](#)[Full Screen / Esc](#)[Printer-friendly Version](#)[Interactive Discussion](#)

POST: turbulent mixing across capping inversion

S. P. Malinowski et al.

Title Page

Abstract

Introduction

Conclusions

References

Tables

Figures

◀

▶

◀

▶

Back

Close

Full Screen / Esc

Printer-friendly Version

Interactive Discussion

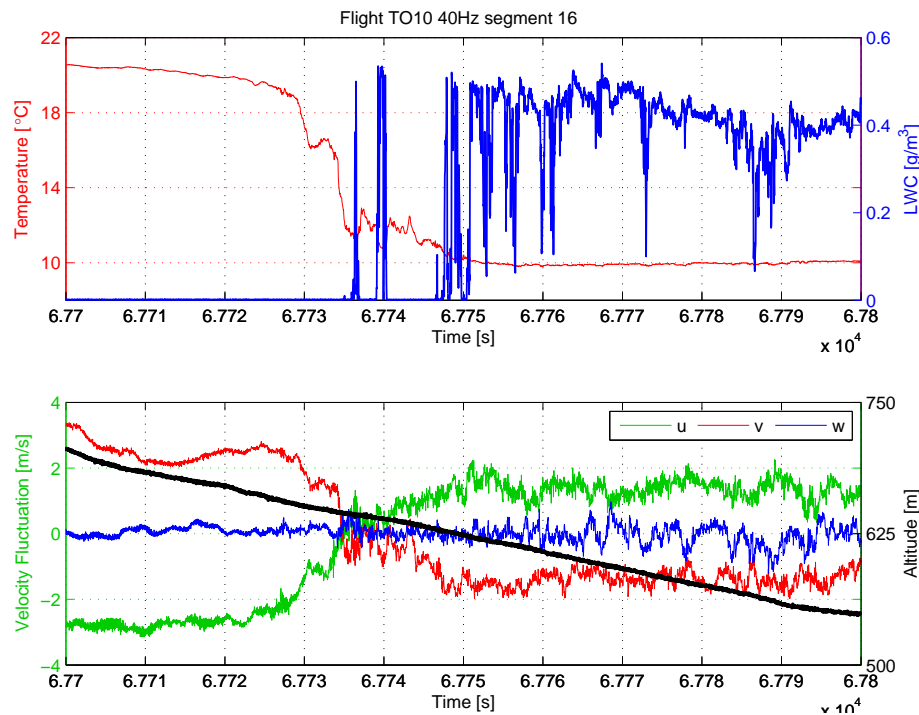


Fig. 3. Temperature T , liquid water content LWC, and velocity fluctuations (mean values subtracted) in the course of a descent into the stratocumulus cloud deck, illustrated by the altitude (black line), during flight TO10.

POST: turbulent mixing across capping inversion

S. P. Malinowski et al.

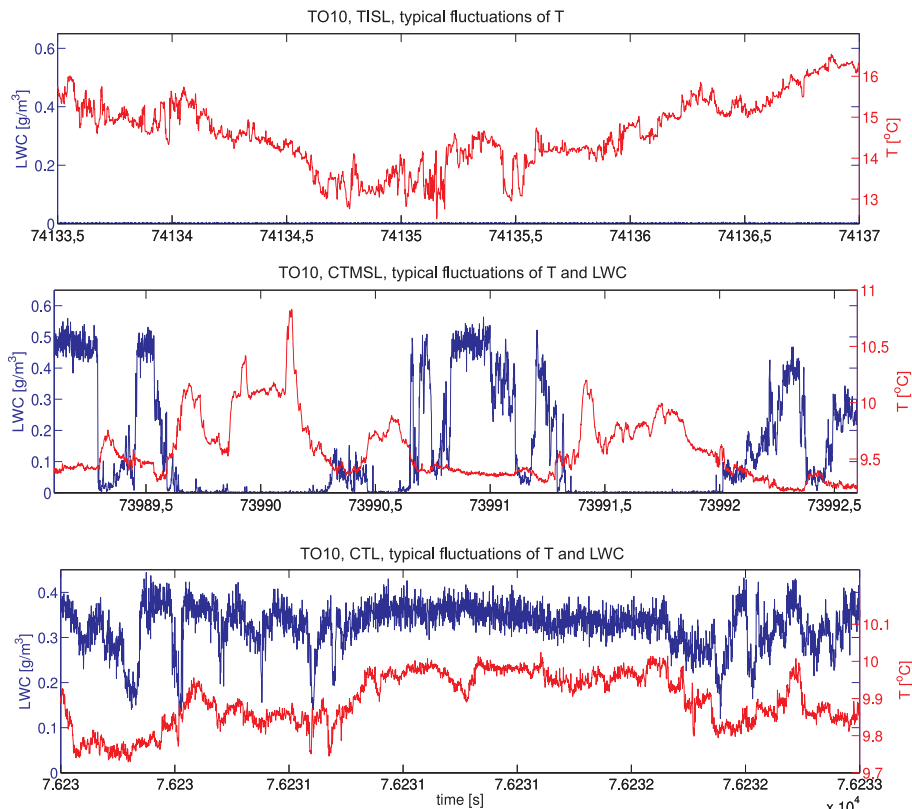


Fig. 4. Typical high resolution (~ 5.5 cm) records of temperature and LWC fluctuations in TISL (upper panel), CTMSL (middle panel) and CTL (bottom panel) from flight TO10.

Title Page

Abstract

Introduction

Conclusions

References

Tables

Figures

◀

▶

◀

▶

Back

Close

Full Screen / Esc

Printer-friendly Version

Interactive Discussion



POST: turbulent mixing across capping inversion

S. P. Malinowski et al.

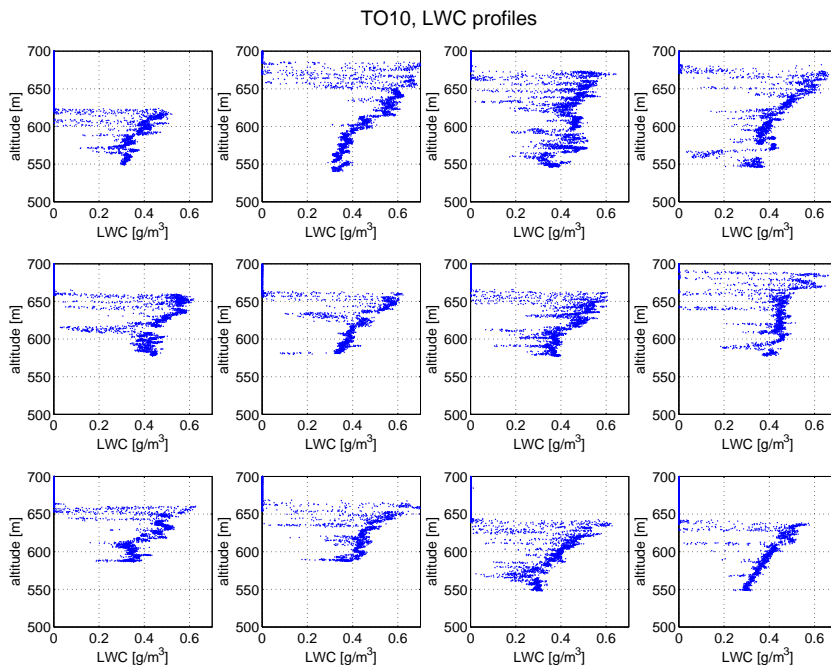


Fig. 5. Typical profiles of LWC collected on porpoises in flight TO10. Each point corresponds to a 1.4 m average (40 Hz data). Four consecutive profiles are shown in each row. Successive rows are from different flight legs in order to illustrate variability of LWC for the whole flight.

[Title Page](#)[Abstract](#)[Introduction](#)[Conclusions](#)[References](#)[Tables](#)[Figures](#)[◀](#)[▶](#)[◀](#)[▶](#)[Back](#)[Close](#)[Full Screen / Esc](#)[Printer-friendly Version](#)[Interactive Discussion](#)

POST: turbulent mixing across capping inversion

S. P. Malinowski et al.

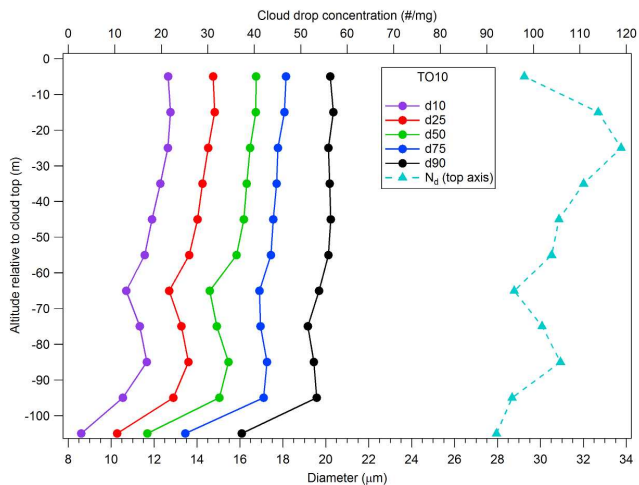


Fig. 6. Vertical profiles of droplet number concentration (triangles, blue, upper axis) and percentiles of droplet size distribution (circles) as a function of altitude relative to cloud top (binned to 10 intervals). Measurements from the phase-Doppler interferometer during TO10.

Title Page

Abstract

Introduction

Conclusions

References

Tables

Figures

◀

▶

◀

▶

Back

Close

Full Screen / Esc

Printer-friendly Version

Interactive Discussion



POST: turbulent mixing across capping inversion

S. P. Malinowski et al.

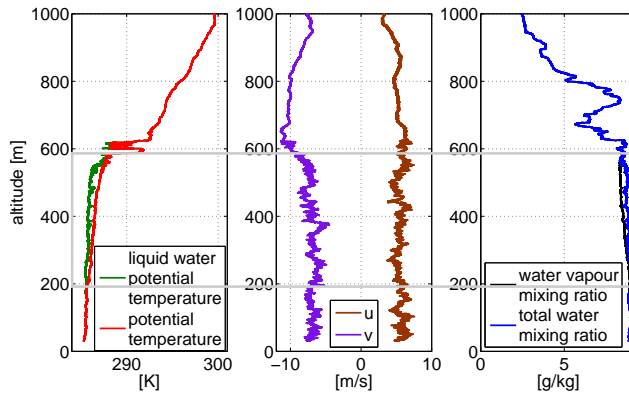


Fig. 7. As in Fig. 2, but for flight TO13.

Title Page

Abstract

Introduction

Conclusions

References

Tables

Figures

◀

▶

◀

▶

Back

Close

Full Screen / Esc

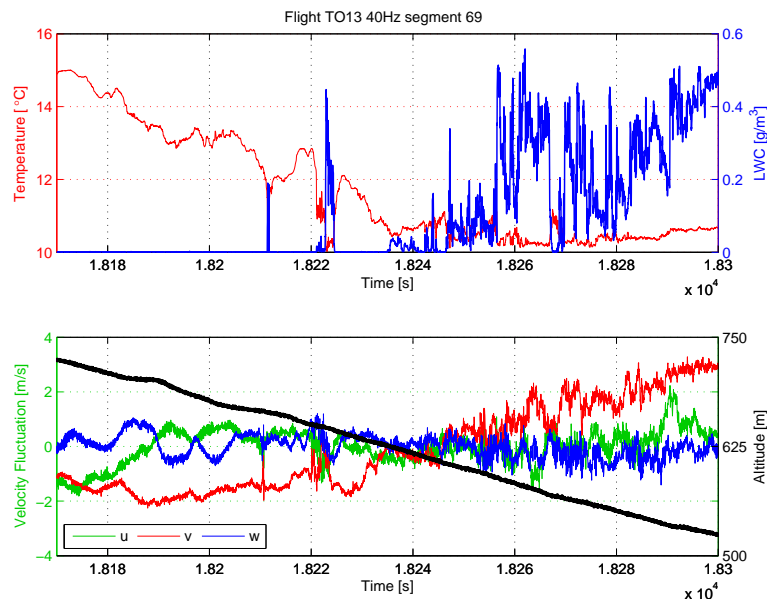
Printer-friendly Version

Interactive Discussion



POST: turbulent mixing across capping inversion

S. P. Malinowski et al.

**Fig. 8.** As in Fig. 3, but for flight TO13.

Title Page

Abstract

Introduction

Conclusions

References

Tables

Figures

◀

▶

◀

▶

Back

Close

Full Screen / Esc

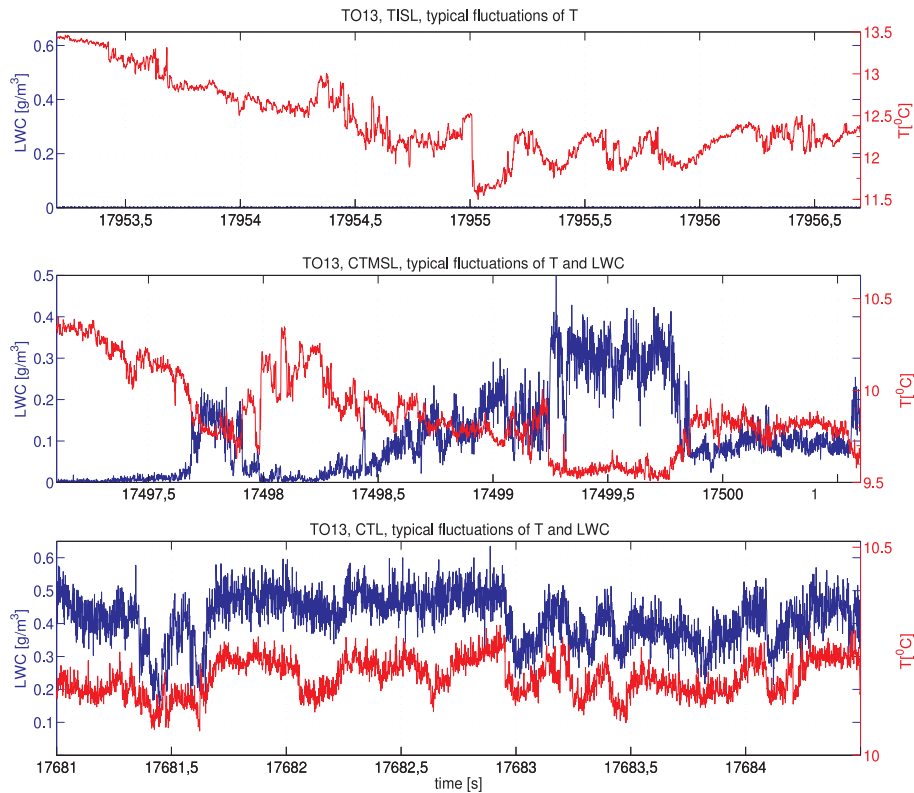
Printer-friendly Version

Interactive Discussion



POST: turbulent mixing across capping inversion

S. P. Malinowski et al.

**Fig. 9.** As in Fig. 4, but for flight TO13.

Title Page

Abstract

Introduction

Conclusions

References

Tables

Figures

◀

▶

◀

▶

Back

Close

Full Screen / Esc

Printer-friendly Version

Interactive Discussion



POST: turbulent mixing across capping inversion

S. P. Malinowski et al.

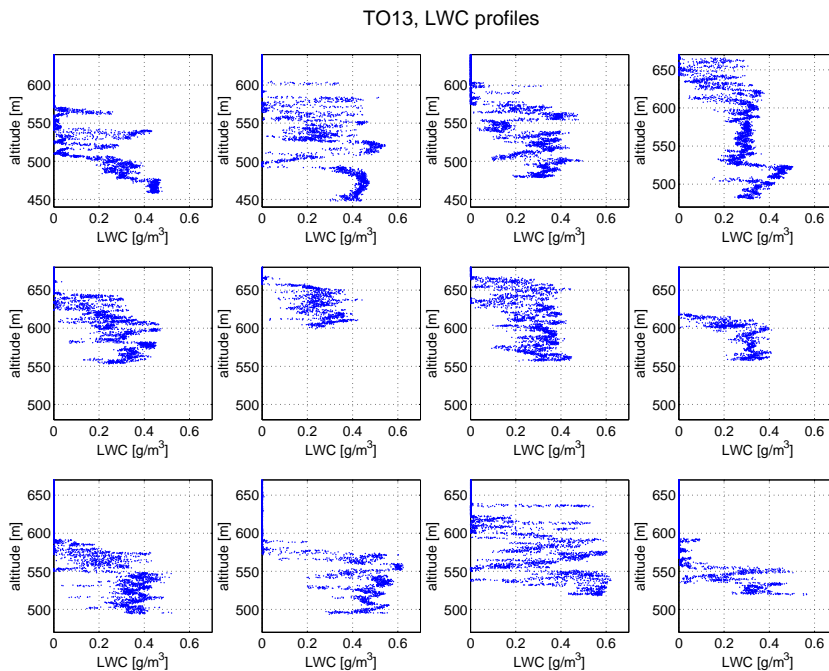


Fig. 10. As in Fig. 5, but for TO13 flight.

Title Page

Abstract

Introduction

Conclusions

References

Tables

Figures

◀

▶

◀

▶

Back

Close

Full Screen / Esc

Printer-friendly Version

Interactive Discussion



POST: turbulent mixing across capping inversion

S. P. Malinowski et al.

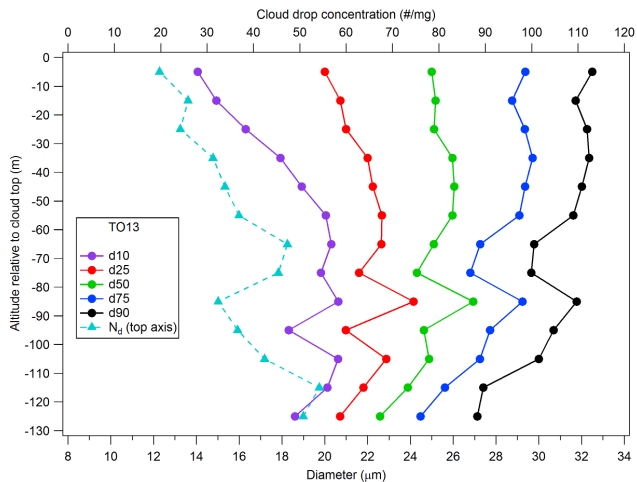


Fig. 11. As in Fig. 6, but for flight TO13.

Title Page

Abstract

Introduction

Conclusions

References

Tables

Figures

◀

▶

◀

▶

Back

Close

Full Screen / Esc

Printer-friendly Version

Interactive Discussion



POST: turbulent mixing across capping inversion

S. P. Malinowski et al.

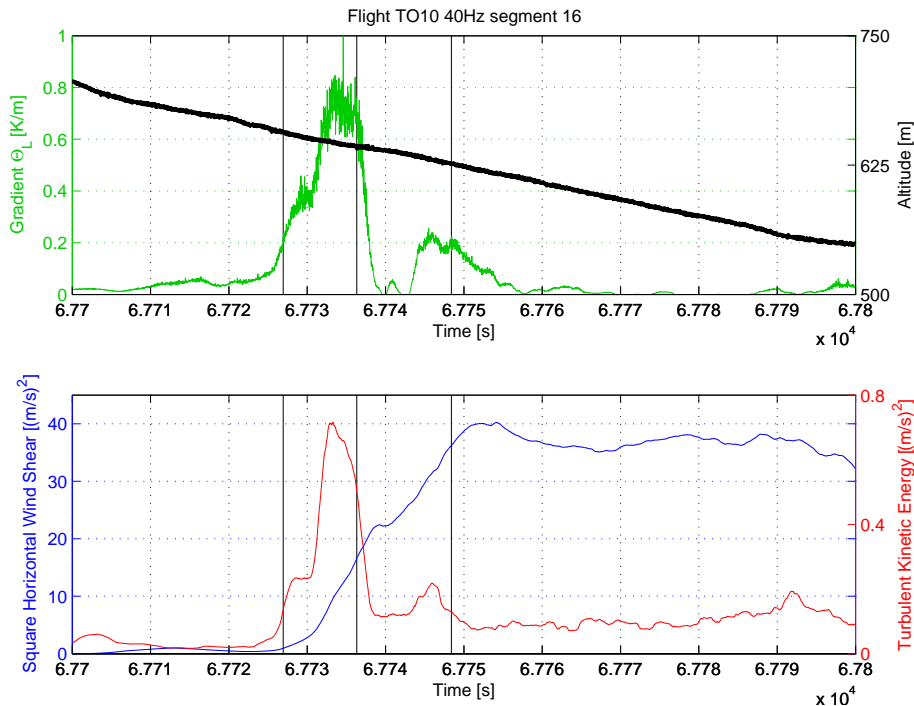


Fig. 12. Gradient of the liquid water potential temperature, horizontal wind, and turbulent kinetic energy for the same descending segment of flight TO10 shown in Fig. 3. Three black vertical lines mark borders between the free troposphere, the inversion, the cloud mixing layer and the cloud top.

[Title Page](#)[Abstract](#)[Introduction](#)[Conclusions](#)[References](#)[Tables](#)[Figures](#)[◀](#)[▶](#)[◀](#)[▶](#)[Back](#)[Close](#)[Full Screen / Esc](#)[Printer-friendly Version](#)[Interactive Discussion](#)

POST: turbulent mixing across capping inversion

S. P. Malinowski et al.

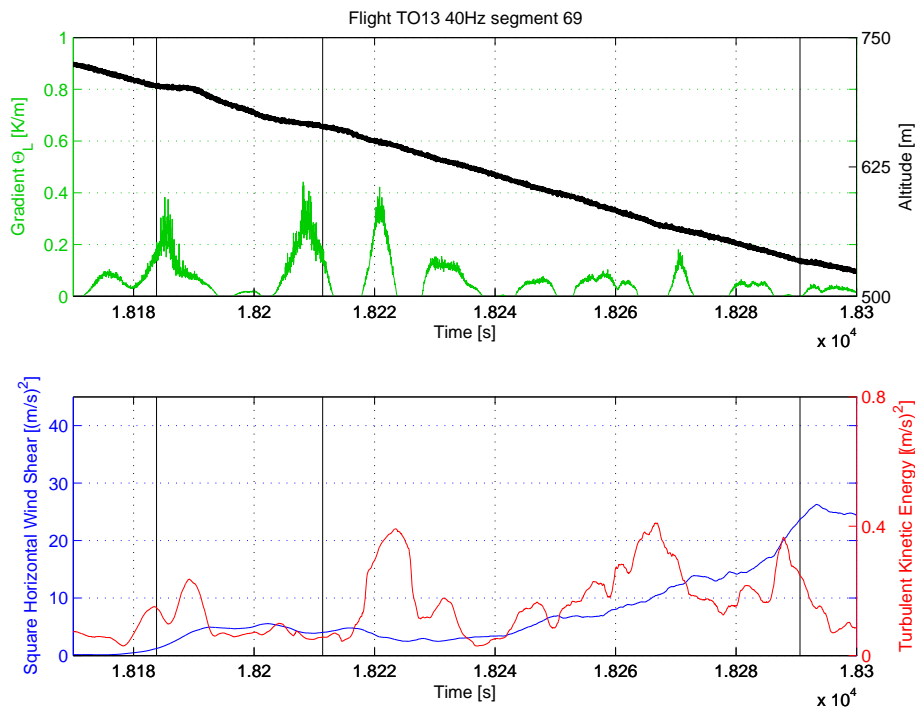


Fig. 13. As in Fig. 12, but for flight TO13. The flight segment corresponds to Fig. 8.

[Title Page](#)[Abstract](#)[Introduction](#)[Conclusions](#)[References](#)[Tables](#)[Figures](#)[◀](#)[▶](#)[◀](#)[▶](#)[Back](#)[Close](#)[Full Screen / Esc](#)[Printer-friendly Version](#)[Interactive Discussion](#)

POST: turbulent mixing across capping inversion

S. P. Malinowski et al.

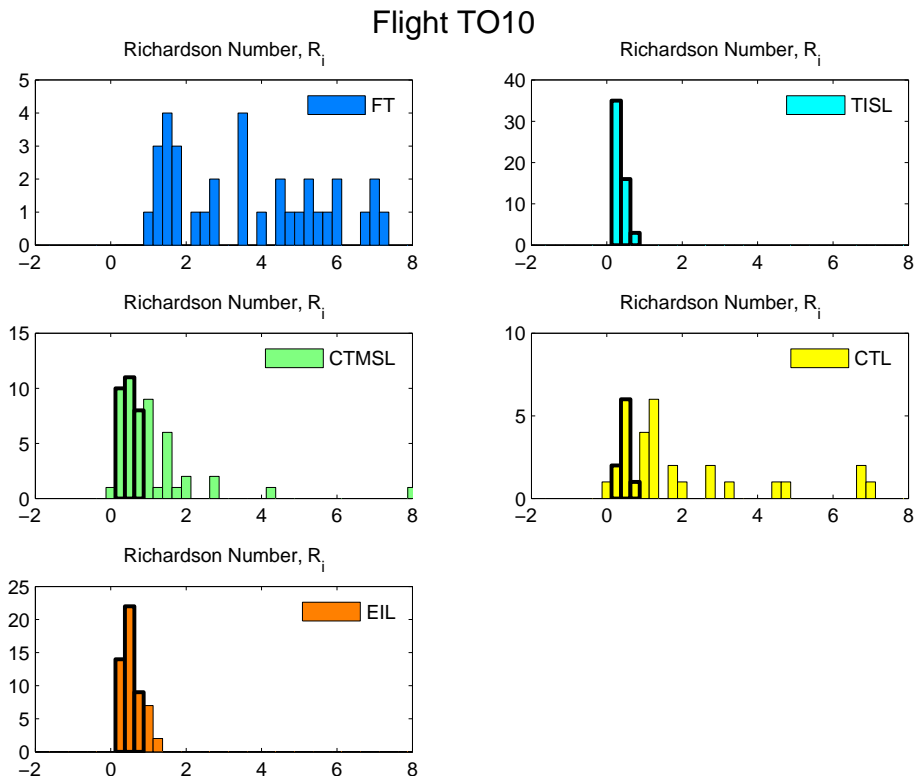


Fig. 14. Distribution of observed Richardson number in each layer for different porpoises in flight TO10. The heavy black lines highlights the critical bins centered on $R_i = [0.25, 0.5, 0.75]$.

Title Page

Abstract

Introduction

Conclusions

References

Tables

Figures

⏪

⏩

◀

▶

Back

Close

Full Screen / Esc

Printer-friendly Version

Interactive Discussion



POST: turbulent mixing across capping inversion

S. P. Malinowski et al.

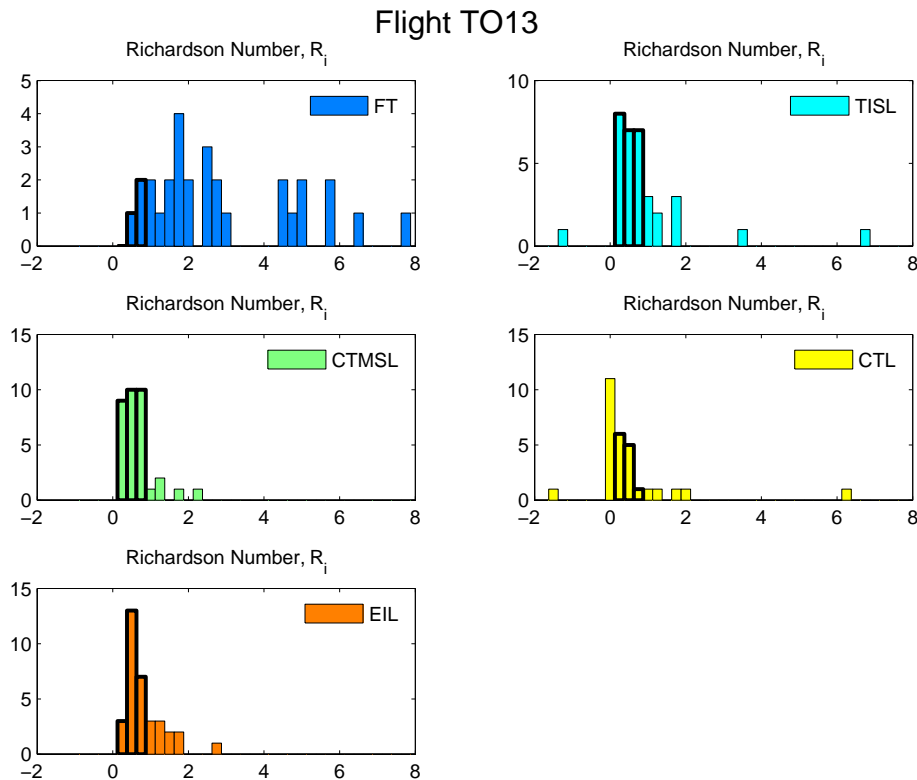


Fig. 15. As in Fig. 14, but for flight TO13.

Title Page

Abstract

Introduction

Conclusions

References

Tables

Figures

⏪

⏩

◀

▶

Back

Close

Full Screen / Esc

Printer-friendly Version

Interactive Discussion



POST: turbulent mixing across capping inversion

S. P. Malinowski et al.

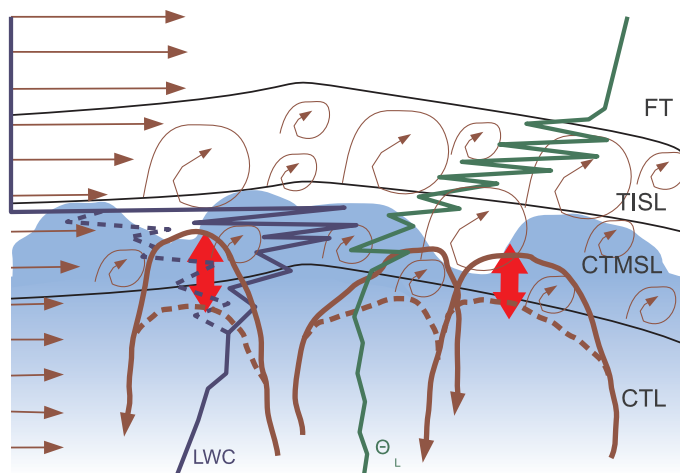


Fig. 16. Cartoon summarizing the main physical mechanisms of mixing in stratocumulus top: FT – free troposphere, TISL – turbulent inversion sublayer, CTMSL – cloud top mixing sublayer (TISL + CTMSL = EIL – entrainment interface layer), CTL – cloud top layer, straight brown arrows – mean wind, thin spiral brown arrows – turbulent eddies due to shear, thick brown curved arrows – convective eddies in the boundary layer, green and blue lines – schematic θ_1 and LWC profiles from airborne measurements, the red double arrows indicate buoyancy sorting in EIL. Solid lines correspond to “typical” CTEI permitting situation, while dashed lines show differences in “non-typical” CTEI prohibiting situation.

Title Page

Abstract

Introduction

Conclusions

References

Tables

Figures

◀

▶

◀

▶

Back

Close

Full Screen / Esc

Printer-friendly Version

Interactive Discussion

